Journal of Physics: Conference Series **2156** (2022) 012022 doi:10.1088/1742-6596/2156/1/012022

Characterization of an ultra-high purity NaI(Tl) crystal scintillator with the SABRE Proof-of-Principle detector

A. Mariani[1,2] on behalf of the SABRE Collaboration

[1] Physics Department, Princeton University, Princeton, NJ 08544, USA
[2] INFN - Laboratori Nazionali del Gran Sasso, Assergi (L'Aquila) I-67100, Italy

E-mail: am8894@princeton.edu

Abstract. The SABRE experiment aims to detect the annual modulation of the dark matter interaction rate by means of ultra-high purity NaI(Tl) crystals. It focuses on the achievement of a very low background to carry out a model-independent and high sensitivity test of the long-standing DAMA result. SABRE has recently completed a Proof-of-Principle (PoP) phase at the Gran Sasso National Laboratory, devoted to assess the radiopurity of the crystals. The results on the radiopurity of a 3.4-kg NaI(Tl) crystal scintillator grown within the SABRE Collaboration and operated underground in the SABRE-PoP setup, will be reported and discussed. The amount of potassium content in the crystal, determined by direct counting of ^{40}K, is found to be < 4.7 ppb at 90% CL. The average background rate in the 1-6 keV energy region of interest (ROI) is 1.20 ± 0.05 counts/day/kg/keV, which is, for the first time, comparable with DAMA/LIBRA-phase1. Our background model indicates that this rate is dominated by ^{210}Pb, and that about half of this contamination is located in the PTFE reflector wrapped around the crystal. Ongoing developments aimed at a further reduction of radioactive contaminants in the crystal indicates that a background rate ≤ 0.3 counts/day/kg/keV in the ROI is within reach. This value represents a benchmark for the development of next-generation NaI(Tl) detector arrays for the direct detection of dark matter particles.

1. Introduction

SABRE (Sodium-iodide with Active Background REjection) is an experiment based on NaI(Tl) scintillating crystals and focused on the achievement of an ultra-low background to search for galactic dark matter through the annual modulation effect, and test in a model-independent way and with high sensitivity the long-standing DAMA result. Indeed, an annually modulated signal compatible with the dark matter hypothesis has been observed with very high statistical significance in the 2-6 keV (phase 1), and later in the 1-6 keV (phase 2) energy region, by the DAMA/LIBRA experiment operating an array of 250 kg of high purity NaI(Tl) crystals at the Gran Sasso National Laboratory (LNGS) [1]. Experiments using different target materials seem to exclude the interpretation of the DAMA signal as due to spin-independent dark matter scattering off nuclei in the standard WIMP galactic halo hypothesis [2]. On the other hand, currently running experiments using the same target, such as ANAIS and COSINE [3, 4], have not yet reached the ultra-low background and sensitivity achieved by DAMA. For this reason, a new high sensitivity and low background measurement with NaI(Tl) crystals is needed.

2. SABRE NaI(Tl) crystals

Low background can be achieved through the development of ultra-high purity NaI(Tl) crystals. Indeed, the main background is due to crystal internal contaminants [1, 5, 6]. Several years of R&D [7, 8] have led to the successful growth of two crystals with masses of 3 and 3.4 kg, denoted as NaI-31 and NaI-33, respectively. Both crystals were grown at RMD (Radiation Monitoring Devices) with ultra-pure Astrograde NaI powder and using the Vertical Bridgman method [9]. Samples from tip and tail were sent to Seastar Chemicals for ICP-MS measurements. From the concentration of ^{39}K we estimated the average $^{\mathrm{nat}}$K contamination in the crystals, which was found to be 17.7 ppb for NaI-31 and 4.6 ppb for NaI-33 [8, 10]. The former is at the same level of DAMA, and ANAIS and COSINE best crystals [1, 5, 6], while the latter is the lowest level ever achieved for NaI(Tl) crystals.

A first crystals characterization underground was performed in a passive shielding setup in Hall B at LNGS [11]. Light yield and energy resolution, measured with a ^{241}Am source at the 59.5 keV γ line, were found to be 12.1 (9.1) phe/keV and 13% (14%), respectively, for the NaI-33 (NaI-31) crystal. ^{238}U and ^{232}Th contents are fully compatible with the SABRE target ($<$ 1 ppt). The alpha rates instead, evaluated using pulse shape discrimination techniques and equal to 1.02 $\pm$ 0.07 mBq/kg and 0.54 $\pm$ 0.01 mBq/kg for the NaI-31 and NaI-33 crystals, respectively, are higher than DAMA, but lower than ANAIS and COSINE crystals [1, 5, 6]. It should be noted that, in both SABRE crystals, alpha rates are mostly due to ^{210}Po from a ^{210}Pb contamination out of equilibrium.

3. Measurements with the SABRE Proof-of-Principle detector

To fully characterize the SABRE crystals and evaluate the potassium content, we used the more sensitive SABRE Proof-of-Principle setup, equipped with a liquid scintillator (LS) active veto. The SABRE-PoP is located in Hall C at LNGS, and its goal is to assess the radiopurity of the crystals and test the active veto performance. In this phase, we operate one SABRE detector module at a time, whose design, together with that of the whole setup, is described in detail in Ref. [12]. The SABRE-PoP was commissioned between May and July 2020 and took data until September 2020, before being stopped due to technical maintenance. Despite the short acquisition time, we obtained several important results.

3.1. Potassium direct counting

A coincidence analysis between crystal and veto detector was performed to evaluate the potassium content in SABRE crystals. To identify the ^{40}K signal, we require: a crystal energy deposition within $\pm 1\sigma_C$ around the 3.2 keV peak and a veto energy deposition within $\pm 2\sigma_V$ around the 1461 keV γ peak, where σ_C and σ_V are the energy resolution of crystal and veto, respectively. The efficiency of the selection, calculated by Monte Carlo, was taken into account in the analysis. Fig. 1 shows the energy deposited in the LS veto versus the energy deposited in the crystal for both the NaI-31 (left) and NaI-33 (right) detectors. The accumulation of events due to the electron capture decay of ^{40}K is clearly visible in the signal band for the NaI-31 crystal due to its greater amount of potassium. The two sidebands, adjacent to the signal band, were used to subtract accidental coincidences. Fig. 2 shows the veto energy spectra in the three different crystal energy bands for both NaI-31 (left) and NaI-33 (right). As expected, the 1461 keV γ peak of ^{40}K is visible only in the signal band, shown in black, especially for the NaI-31 crystal. Fig. 3 shows instead the crystal energy spectrum by requiring coincidences with veto in the signal band. The results obtained are reported in Tab. 1. Given the limited statistics of the measurement, for the NaI-33 crystal we also estimated an upper limit: the ^{40}K activity is $<$ 0.15 mBq/kg, which corresponds to a $^{\mathrm{nat}}$K contamination $<$ 4.7 ppb at 90% CL [13]. This analysis has demonstrated that the PoP setup is sensitive to a ppb-level contamination of K

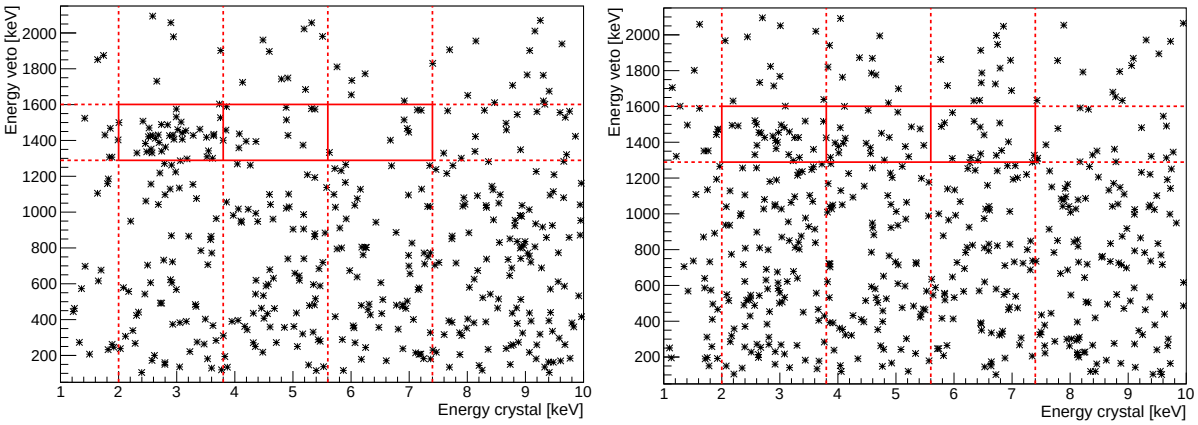

Figure 1. Energy deposited in the LS veto versus energy deposited in the crystal, for the NaI-31 (left) and NaI-33 (right) detectors. The three energy windows used for the analysis (signal band + two sidebands) are also indicated with red solid lines. The exposure collected is ∼60 kg·days for the NaI-31 and ∼90 kg·days for the NaI-33.

in the crystal and, more importantly, that results from direct counting are in agreement with ICP-MS measurements from crystal samples.

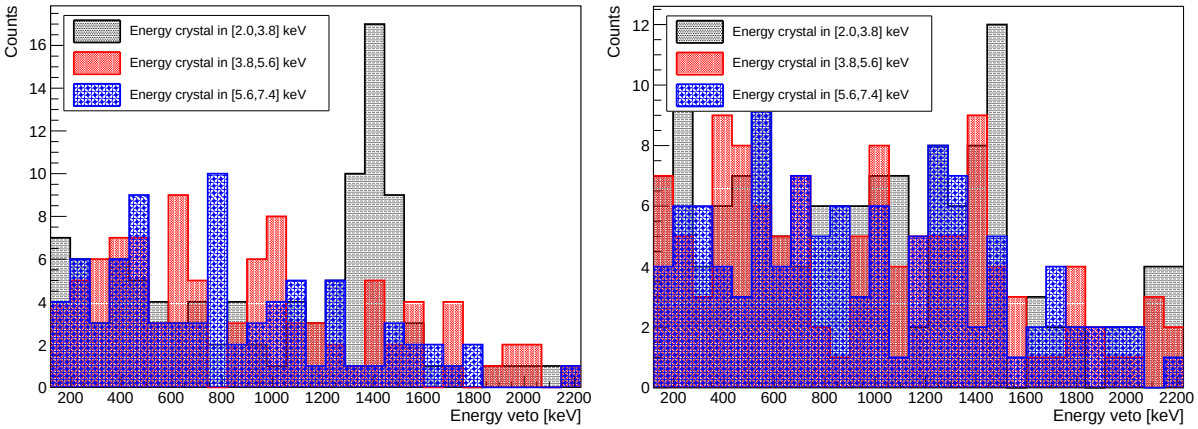

Figure 2. Veto energy spectra obtained by selecting the crystal energy in the three different bands for both NaI-31 (left) and NaI-33 (right) [13].

	NaI-31	**NaI-33**
^{40}K activity [mBq/kg]	0.49 ± 0.10	0.07 ± 0.05
^{nat}K contamination [ppb]	15.7 ± 3.2	2.2 ± 1.5
^{nat}K contamination by ICP-MS [ppb]	17.7 ± 1.1	4.6 ± 0.2

Table 1. Summary of the results of the potassium analysis for the two SABRE crystals [13].

3.2. NaI-33 low energy data analysis and background model

In this section, we report the low energy data analysis performed for the NaI-33 crystal, which is the SABRE best performing crystal. To reject coincident backgrounds, events with energy larger

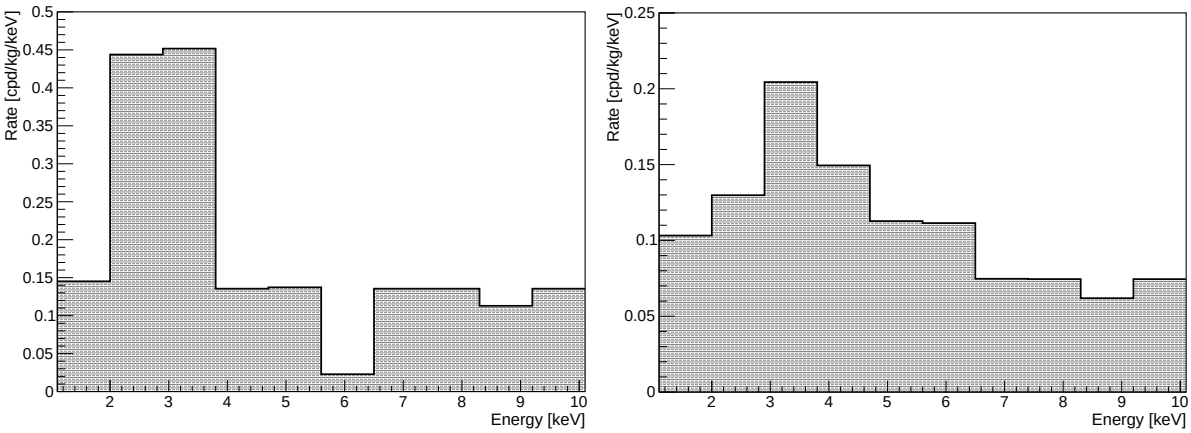

Figure 3. Energy spectra of NaI-31 (left) and NaI-33 (right) crystals obtained by requiring coincidences with veto in the ^{40}K signal band [13].

than 50 keV in the veto are rejected with 42% veto rejection power in the ROI. In addition, to reduce noise at very low energies, the selection criteria (cuts) described in Ref. [14] were applied. The average event acceptance in the ROI, estimated using a calibration run with a ^{228}Th source, is 77.6% [13]. The energy spectrum after cuts and efficiency correction is shown in Fig. 4 (black dots) up to 100 keV (left) and up to 20 keV (right). The measured rate in 1-6 keV is 1.20 ± 0.05 cpd/kg/keV.

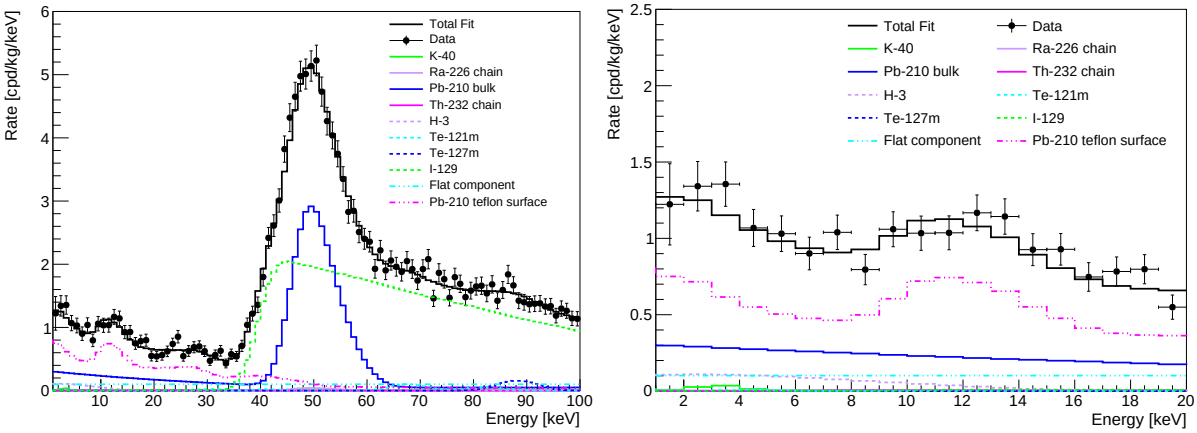

Figure 4. Energy spectrum of the NaI-33 crystal up to 100 keV (left) and up to 20 keV with a spectral fit. The spectra are shown after noise rejection and efficiency correction.

A spectral analysis was performed to quantify the contribution of different background components and build the background model of the NaI-33 crystal [13]. Predicted spectral shapes from different background sources were calculated by Monte Carlo [15]. The result of the best-fit ($\chi^2/N_{dof} = 96/88$) is superimposed in Fig. 4. Tab. 2 reports the activities of the different background components in the NaI-33 crystal determined from the spectral fit (2nd column) and the current rate in ROI (3rd column). The dominant background contributions are from a ^{210}Pb contamination in the PTFE reflector wrapped around the crystal and a ^{210}Pb contamination in the crystal bulk.

Source	**Activity in NaI-33 [mBq/kg]**	**Rate in ROI in NaI-33 [cpd/kg/keV]**	**Projected rate in ROI [cpd/kg/keV]**
^{40}K	0.14±0.01	0.018±0.001	≤0.004
^{210}Pb (bulk)	0.41±0.02	0.28±0.01	≤0.093±0.003
^{226}Ra	0.0059±0.0006	0.0044±0.0005	0.0044±0.0005
^{232}Th	0.0016±0.0003		
^{3}H	0.012±0.007	≤0.12	≤0.12
^{129}I	1.34±0.04		
^{121m}Te	≤0.084	≤0.011	≤0.011
^{127m}Te	0.016±0.006		
^{210}Pb (PTFE)	0.32±0.06	0.63±0.09	≤0.007
Other		0.10±0.05	0.10±0.05
total		1.16±0.10	0.33±0.05

Table 2. Background components in NaI-33 from the spectral fit, current and projected rate in ROI (1-6 keV) for future NaI(Tl) crystals. The future rate assumes zone refining purification and improved reflector radiopurity. The activity of ^{210}Pb in the reflector is normalized to the crystal mass for comparison with bulk activities. Upper limits are given as one-sided 90% CL. Rates are conservatively calculated using upper limits.

4. Conclusions and future perspectives

The SABRE-PoP has concluded its data taking by demonstrating a background level of ∼1.2 cpd/kg/keV in the 1–6 keV ROI, operating the NaI-33 crystal inside the LS active veto. This result represents a breakthrough in terms of radiopurity after the DAMA/LIBRA experiment. Thanks to our background model, we have identified the main background sources, namely the ^{210}Pb contamination in the crystal bulk and especially in the PTFE reflector wrapped around the crystal. Since we have no evidence that impurities are introduced during the crystal growth, we have tested zone refining (ZR) [16] of ultra-high purity NaI powder to further improve the radiopurity in future SABRE crystals [17]. Results of these tests are reported in Ref. [17]. ^{40}K and ^{87}Rb (from ^{39}K and ^{85}Rb measurements) are reduced to negligible levels, and ^{208}Pb by at least a factor of three. Therefore, we can reasonably assume that ZR should be effective also for ^{210}Pb. Assuming the NaI-33 contamination after scaling for the reduction factors observed in the ZR tests [17] and using a clean PTFE reflector, future SABRE crystals would reach a background rate in the ROI ≤ 0.3 cpd/kg/keV (Tab. 2, 4th column). This rate is mostly due to a ^{210}Pb contamination in the crystal, which could be further reduced by ongoing developments in the crystal manufacture, such as helium purging during the ZR process.

References

[1] Bernabei R. et al. 2020 *Prog. Part. Nucl. Phys.* **114**:103810.
[2] Schumann M. 2019 *J. Phys. G* **46**:103003.
[3] Amaré J. et al. 2021 *Phys. Rev. D 103*:102005.
[4] Adhikari G. et al. 2019 *Phys. Rev. Lett.* **123**:031302.
[5] Amaré J. et al. 2019 *Eur. Phys. J. C* **79**:412.
[6] Adhikari P. 2018 *Eur. Phys. J. C* **78**:490.
[7] Shields E. K. 2015 *Ph.D. thesis* Princeton University.
[8] Suerfu B. 2018 *Ph.D. thesis* Princeton University.
[9] Bridgman P. W. 1925 *Proceedings of the American academy of arts and sciences* **60**:305-383.
[10] Suerfu B. et al. 2020 *Phys. Rev. Research* **2**:013223.
[11] Antonello M. et al. 2020 *Eur. Phys. J. C* **81**:299.
[12] Antonello M. et al. 2019 *Eur. Phys. J. C* **79**:363.
[13] Mariani A. 2021 *Ph.D. thesis* Gran Sasso Science Institute.
[14] Calaprice F. et al. 2021 *Phys. Rev. D* **104**:021302.
[15] Antonello M. et al. 2019 *Astroparticle Physics* **106**:1–9.
[16] Pfann W. G. 1952 *JOM* **4**: 747.
[17] Suerfu B. et al. 2021 *Phys. Rev. Applied* **16**:014060.